Micellar Shape and Long-Range-Ordering Transitions in Ternary Surfactant Solutions

Massimo G. Noro and William M. Gelbart*

Department of Chemistry and Biochemistry, University of California at Los Angeles, Los Angeles, California 90095

Received: April 16, 1997; In Final Form: June 24, 1997[⊗]

We treat the competition between *self-energy* (*single*-micelle curvature preference) and *interaction* (*inter*aggregate) effects on the evolution of micellar shapes and long-range ordering phase transitions in ternary systems of mixed surfactant and water. One surfactant prefers to satisfy the hydrophobic effect via formation of globular (positive curvature) micelles, whereas for the other we have in mind the phospholipids, for instance, which prefer to aggregate as planar bilayers. It follows that the preferred curvature in the ternary mixture case will depend sensitively on composition, *i.e.*, on the relative numbers of the two surfactants. At high total concentrations of surfactant, however, the micellar shape is controlled as well by the relative efficiencies of packing aggregates of different curvature, independent of relative amphiphile mole numbers. By combining these self-energy and intermicellar interaction effects, then, we are able to generate "master" phase diagrams for the ternary systems, as a function of composition and concentration.

I. Introduction

During the past 20 years there has been a tremendous range of fundamental research efforts devoted to the study of aqueous solutions of micellized surfactant.[1−3] In the case of dilute solutions, where the surfactant concentration is just above the threshold ("cmc") for micelle formation, both theoretical and experimental investigations have focused on the issue of preferred micellar *shape*. More explicitly, when each micelle is essentially independent of all of the others, will it comprise a globular ("spherical"), prolate ("rodlike"), or oblate ("disklike") aggregate of surfactant molecules? Examples of each kind are now well-documented: C_8E_{12} strongly prefers globular micelles; SDS and CTAB form short and long rods, respectively; CsPFO forms small disklike micelles; phospholipids are well-known to organize spontaneously into extended bilayers ("large disks"), and similarly for hundreds of other amphiphilic molecules. These short-range, molecular-packing preferences have been variously accounted for in terms of the relative lateral areas required by the "head" and "tail" portions of the amphiphiles. A combination of big heads and short tails implies that the hydrophobic effect is best satisfied via positive curvature, hence globular/spherical micelles. Conversely, smaller heads and longer (or double) tails imply less positive curvature, e.g., cylindrical, disklike, bilayer, or—ultimately—*inverted* micellar organization. We shall refer to these single-micelle considerations as *self-energy* effects. In addition to the discussions already cited,[1−3] many recent papers have addressed these molecular statistical mechanical aspects of spontaneous micellization and subsequent evolution of size and shape upon an increase in concentration: see, for example, refs 4−6 and papers cited therein.

At higher concentrations, the volume fraction of micelles is no longer negligible and *interactions* between the aggregates become important. In many instances, a phase transition is observed from an isotropic solution of globular micelles to a hexagonal phase of cylinders or from rodlike micelles to a lamellar state of bilayers, etc. Clearly, the self-energy effects are being overwhelmed here by the *inter*aggregate interactions, and the short-range, molecular-packing preferences are sacrificed in order to reduce the intermicellar free energy. As argued elsewhere[7] for binary (surfactant in water) systems, and as featured below in the context of ternary aqueous solutions of two different surfactants, the change in micellar shape comes about largely because of purely geometric packing considerations. That is, high-curvature (*e.g.*, spherical) colloidal particles do not pack as efficiently as lower-curvature ones (cylinders and sheets). This is most dramatically pointed up by the fact that "hard" spheres can only fill up 74% of the available volume—and they reach this limit only upon close packing into a hexagonal lattice—whereas cylinders can align and hexagonally pack up to 91% volume fraction and sheets up to 100%.[7] In this way one can understand the transition from isotropic solution of micellar spheres to hexagonal and lamellar phases of cylinders and bilayers, respectively, upon an increase in the overall concentration of the amphiphile. The role of interaggregate excluded volume in shape and long-range-ordering transitions in micellar solutions has been developed most systematically by Herzfeld *et al*.[8] An earlier approach[9,10] had treated specifically the relative importance of intra- and interaggregate *electrostatic* interactions in driving the hexagonal → lamellar phase change in lipid systems, with[10] and without[9] alcohol cosurfactant.

In the case of mixtures of surfactants, the situation is necessarily more complicated. We have already noted that some amphiphiles strongly prefer to form small globular (high-positive-curvature) micelles at the cmc, while others organize directly into planar bilayers. It is clear, then, that a dilute aqueous solution of a mixture of two such surfactants will be composed of globular micelles, or bilayers—or aggregates of some intermediate curvature—according to the relative numbers of the two amphiphiles. Accordingly, we expect to see an evolution of micellar shape, from high to low curvature, for example, upon increasing the mole fraction of a phospholipid-like (planar-bilayer-loving) component relative to that of the curvature-loving amphiphile. This is much the same evolution that we referred to just above, in our discussion of sphere → rod → sheet evolution in single-surfactant-in-water systems upon an increase in concentration. It follows that in ternary systems of "surfactant" plus "phospholipid" plus water, the progression of micellar shape and long-range-ordering transitions will be driven by a delicate balance between composition and concentration effects. We shall see below that those arguments can

[⊗] Abstract published in *Advance ACS Abstracts,* September 15, 1997.

S1089-5647(97)01329-1 CCC: $14.00

explain the trends in the collection of experimental ternary phase diagrams compiled by Ekwall.[11]

In the present work we provide a simple formulation of the competing effects of self-energy and intermicellar interaction effects, as a function of composition and concentration, in aqueous solutions of curvature-loving and planar-bilayer-loving amphiphiles. Throughout our analysis the curvature-loving species will be referred to as the "surfactant" (S), even though the term surfactant is generally used for *any* surface-active/micelle-forming amphiphile, regardless of its curvature preference. Similarly, the bilayer-forming component will be labeled as "lipid" (L), despite the fact that certain *non*-lipid species are also known to organize as bilayers in aqueous solution. To treat the self-energy contributions, we simply consider the two (standard free) energy differences $\epsilon^{hex} - \epsilon^{lam}$ and $\epsilon^{mic} - \epsilon^{lam}$ for each species S and L, with typical values for these quantities chosen from earlier theories which treat explicitly the short-range molecular packing involving head groups and semiflexible tails in micellar environments of different curvature. [The superscripts "hex", "lam", and "mic" denote hexagonal (cylinder), lamellar (bilayer), and micelle (globular/spherical): thus, for example, $(\epsilon^{hex} - \epsilon^{lam})_S$ describes the change in energy as a single "S" molecule is moved from lamellar/bilayer to hexagonal/cylinder environment, etc.] We emphasize that our idea here is not to provide any quantitative, *a priori*, descriptions but rather to predict *qualitatively* a broad range of structural evolutions and phase behaviors in ternary solutions involving two types ("S" and "L") of amphiphile. In this same spirit we treat the inter-aggregate interactions by introducing hard particle forces between the micellar structures. While "soft", distance-dependent repulsions and attractions between aggregates are certainly operative in real systems, we argue that the excluded-volume forces which we consider are nevertheless sufficient to capture the essence of the coupling between self-energy and intermicellar interaction effects.

In section II we illustrate our approach by treating the transition from hexagonal to lamellar phase in concentrated solutions of S *or* L in water. Then, in section III, we mix the S *and* L components and determine the ternary phase diagram for typical sets of self-energy differences for cylindrical and bilayer geometries. Competition between composition and concentration effects is explicitly calculated. Tie lines between the coexisting hexagonal and lamellar phases, for example, indicate the extent to which the hexagonal state is richer in the S component. We also include there the competition of these solution phases with *pure* S and L crystals which separate out at high concentration and with dilute solutions of (S-rich) micelles and (L-rich) vesicles at sufficiently low concentrations.

II. Hexagonal → Lamellar Transitions in Binary Systems

Columnar Phase. As a first approximation for treating the hexagonal phase, we neglect the long-range lateral ordering and model the phase—henceforth referred to alternately as "columnar" and "hexagonal"—as a collection of perfectly aligned, infinitely long cylinders. While no orientational degree of freedom is allowed, the cylinders can translate "laterally" in space as they retain their perfect alignment. Accordingly, since no defects are permitted along the ordering direction, we can treat the cross-section of this system along an orthogonal plane as a collection of hard disks in a 2D (two dimensional) space, as we show in Figure 1. It is known[12] that a good approximate pressure for such a system—over the *full* range of concentration—can be derived from the *y*-expansion ($y = \phi/(1 - \phi)$, where ϕ is the particle volume fraction) truncated at the second term, with the appropriate coefficients following from the first

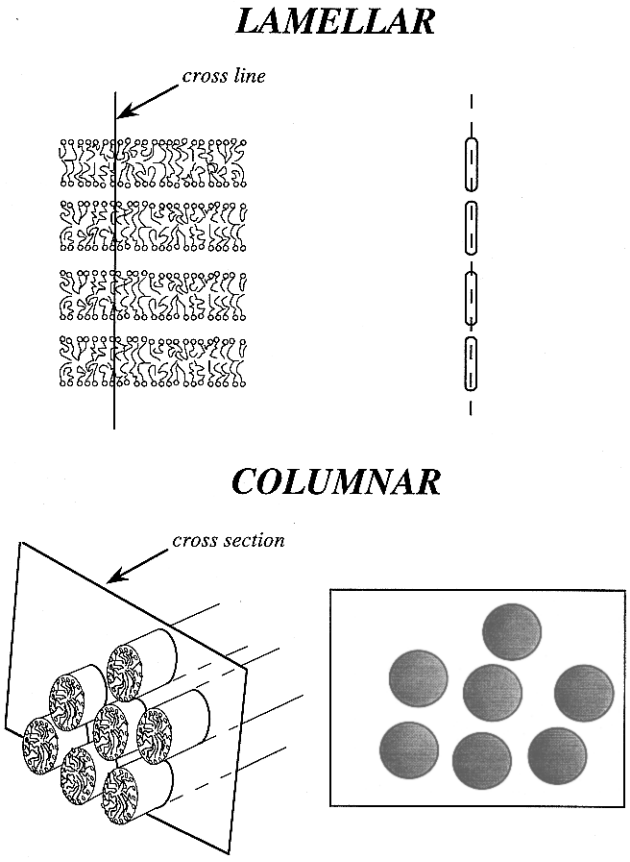

Figure 1. Pictorial transcriptions from 3D lamellar and 3D columnar phases to 1D and 2D packing scenarios, respectively. Note the absence of long-range positional order (see text).

two virial coefficients. More explicitly, we write

$$\frac{Pa}{kT} = \frac{\phi}{1-\phi} + \left(\frac{\phi}{1-\phi}\right)^2 \quad (1)$$

where a is the cross-sectional area of each cylinder and ϕ is the area fraction occupied by the disks. To be precise, we should use a superscript 2D for the area fraction, to distinguish it from the usual ϕ reserved for the overall *volume* fraction. But the area fraction occupied by the disks is the same as the volume fraction occupied by the cylinders, since they are infinitely long and perfectly aligned. Integration of eq 1 gives directly the corresponding free energy per molecule:

$$\frac{F(\phi)}{N} = kT \ln\left(\frac{\Lambda_{cyl}^2}{a}\right) + kT \ln\left(\frac{\phi}{1-\phi}\right) + kT\frac{\phi}{1-\phi} - 2kT \quad (2)$$

where Λ_{cyl} is the De Broglie wavelength of the cylinder. Equation 2 gives the free energy *per object* of a system composed of 2D hard objects in a 2D space. Note that there is no dependence on the *number* of these objects: eq 2 refers to an intensive property of the system. It is true that it was derived for a *cross*-section of the 3D system, but we did not set any constraint on the choice of the particular plane intersecting the cylinders other than that it had to be orthogonal. So the same free energy per disk applies to each section of each cylinder. Now, contained in each section there is a certain number of molecules which, regardless of how many or how they are arranged, move in the 2D space because the whole disk does. Therefore eq 2 also holds for each and every one of the molecules: it is the packing (inter-aggregate) contribution to the free energy per molecule of the columnar phase. Finally, we remark that, whereas we treat here (and below) only *zero-*

range, excluded-volume forces, an inclusion of "soft" repulsions would not change any of our qualitative conclusions.

Lamellar Phase. In this case also we neglect the long-range positional ordering of the bilayers and model this phase as a collection of infinitely large hard slabs, with nonzero thickness. All the slabs are parallel to each other, but the distance between two nearest neighbors does not need to be constant. Only translational degrees of freedom in one dimension are allowed, in the direction orthogonal to the slabs.

We consider then a "line"-section across the slabs and treat them as a collection of 1D objects (rods) in a 1D space (see Figure 1), for which the exact pressure is well-known (Tonk's formula, or—equivalently—a *one*-term truncation of the *y*-expansion):[12]

$$\frac{Pl}{kT} = \frac{\phi}{1-\phi} \tag{3}$$

Here l is the length of each rod, and ϕ is the line fraction, identical to the overall (3D) volume fraction. Integration of eq 3 is carried out, and the free energy per rod becomes

$$\frac{F(\phi)}{N} = kT \ln\left(\frac{\Lambda_{\text{lam}}}{l}\right) + kT \ln\left(\frac{\phi}{1-\phi}\right) - kT \tag{4}$$

where Λ_{lam} is the De Broglie wavelength of the slabs. The same argument as before can be applied to the interpretation of eq 4, and hence it can be regarded as the inter-aggregate (packing) free energy per molecule for the lamellar phase.

Self-Energy. Here we suppress temporarily the inter-aggregate interaction and focus on a single amphiphilic molecule. According to the length of the tail, the polarity (and/or the charge) of the head, etc., it will have a preference toward satisfying the hydrophobic effect via either the cylindrical (hex) or bilayer (lam) local geometry. Suppose we write, for a given amphiphilic species (S or L),

$$F^{\text{hex}}(\phi)/N = \epsilon^{\text{hex}} kT \tag{5}$$

with a similar expression for the lamellar (lam) phase. We expect $|\epsilon^{\text{hex}} - \epsilon^{\text{lam}}|$ to be of the order of unity.[13]

Now, the two contributions to the overall free energy, the inter-aggregate and the intra-aggregate, can be combined together and transformed into a free energy per unit volume and made conveniently dimensionless both in energy and in volume:

$$\tilde{\psi} = \frac{F}{N}\frac{N}{V}\frac{\nu}{kT}F(\phi) \tag{6}$$

where F refers to the $F(\phi)$'s in eqs 2 and 5 and ν is the molecular volume. (For convenience we consider the molecular volume of all three types of molecules present to be the same.)

Water−Surfactant Mixture. A simple case can be analyzed at this point, namely, the two-component limit of the ternary system for which the mole fraction, or volume fraction, of one amphiphile goes to zero. We consider first the W−S (water−surfactant) mixture. The S molecules prefer positive curvature, and we can model this preference by taking the intra-aggregate free energy per molecule of the hexagonal phase to be lower than that of the lamellar phase: $\epsilon^{\text{hex}} < \epsilon^{\text{lam}}$. At low volume fractions, then, the hexagonal phase will appear since the aggregates are far apart and the inter-aggregate interaction is negligible. On the other hand, at high enough volume fractions, the inter-aggregate contribution to the free energy will dominate and the system will eventually become lamellar since bilayers pack better than cylinders, and (see below) the overall free energy of the lamellar phase will become lower than that of the hexagonal phase.

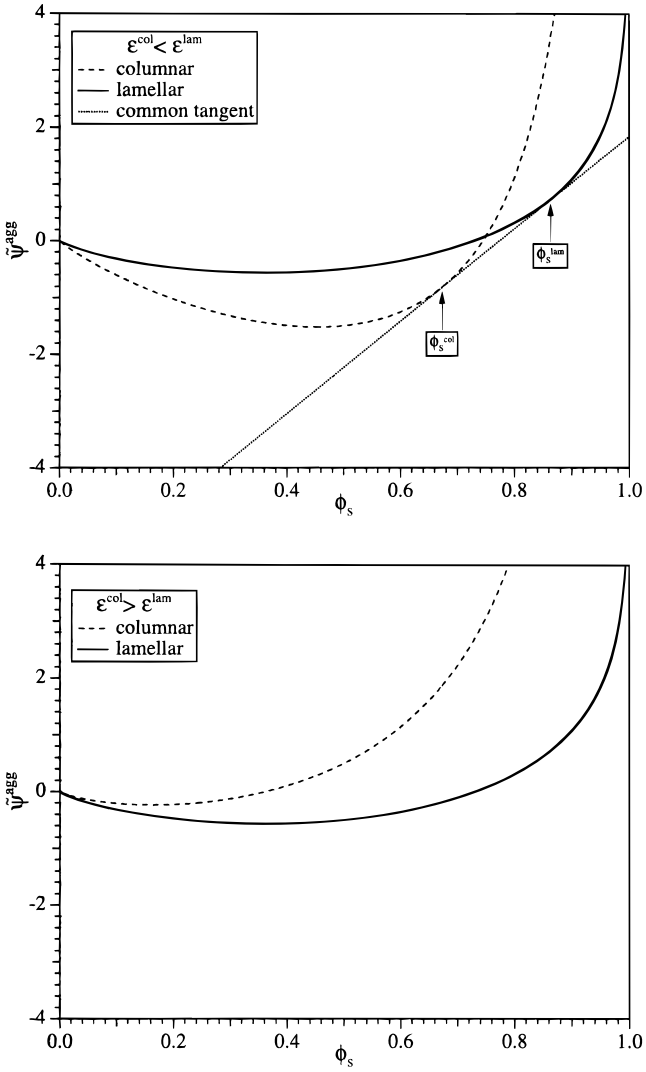

Figure 2. Dimensionless Helmholtz free energy per unit volume $\tilde{\psi}^{\text{agg}}$—see eq 6 in the text—plotted versus volume fraction of surfactant ϕ_S. "Agg" stands for "lam", lamellar phase, and for "col", columnar phase. (a, top) When $\epsilon^{\text{col}} < \epsilon^{\text{lam}}$, there is a region of phase coexistence between the columnar and the lamellar phases, calculated via common tangent construction. (b, bottom) When $\epsilon^{\text{col}} > \epsilon^{\text{lam}}$, there is no phase coexistence.

We employ the usual common tangent construction to determine the two-phase region associated with the transition between hexagonal and lamellar states. It is convenient to work with dimensionless quantities also in this case, the common tangent conditions taking the form[14]

$$\begin{cases} \tilde{\mu}^{\text{lam}}(\phi_S^{\text{lam}}) = \tilde{\mu}^{\text{hex}}(\phi_S^{\text{hex}}) \\ \tilde{p}^{\text{lam}}(\phi_S^{\text{lam}}) = \tilde{p}^{\text{hex}}(\phi_S^{\text{hex}}) \end{cases} \tag{7}$$

where $\tilde{\mu}^{\text{agg}} = \partial\tilde{\psi}^{\text{agg}}/\partial\phi$ is the dimensionless chemical potential and $\tilde{p}^{\text{agg}} = -\tilde{\psi}^{\text{agg}} + \tilde{\mu}^{\text{agg}}\phi$ the dimensionless pressure, with "agg" referring alternatively to "lam" and "hex". Here of course we need to distinguish between ϕ^{hex} and ϕ^{lam}, since the two values represent the volume fractions of amphiphile in the hexagonal and lamellar phases which coexist in equilibrium with one another. The plot of the (dimensionless) free energy density $\tilde{\psi}^{\text{agg}}$ versus the volume fraction ϕ of the amphiphile is shown in Figure 2a, for $\epsilon^{\text{lam}} - \epsilon^{\text{hex}} = 2$. As expected, we see that the inter-aggregate free energy contributions are sufficient at high

volume fraction to overwhelm the self-energy terms, forcing the micellar structures to give up their otherwise (low-concentration) preference for cylindrical geometry in order to pack more efficiently.

Water−Lipid Mixture. Now we consider the W−L (water−lipid) mixture, where the amphiphile (lipid) strongly prefers the lamellar phase at *all* concentrations due to the combined effects of self-energy ($\epsilon^{hex} > \epsilon^{lam}$) and packing contributions. That is, at low volume fractions, the molecules organize themselves into bilayers because this is the best way (without curvature) to satisfy the hydrophobic effect, on a local level (not needing to worry about bumping into other aggregates). Then, at higher concentrations, where inter-aggregate packing considerations become important, the bilayers are *further* favored, since they waste the least space and do the best job of making room for each other. This behavior is evidenced in the plot of $\tilde{\psi}^{agg}$ versus volume fraction shown in Figure 2b, where the hexagonal phase is seen to fall increasingly behind the lamellar state upon concentrating the system.

III. Master Phase Diagram for Ternary Systems

Composition Dependence. So far we have talked exclusively about the limiting cases in which only one kind of amphiphile is present. The extension to a mixed *ternary* system is made at this point.

In order to specify the total concentration and composition of the system, we need the volume fractions ϕ_S, ϕ_L, ϕ_W, satisfying the constraint $\phi_S + \phi_L + \phi_W = 1$. Only two volume fractions can be chosen independently; we find it convenient to choose these 2 degrees of freedom to be the "total concentration"—the total volume fraction of amphiphile $\phi = \phi_S + \phi_L$—and the "composition"—the ratio between the volume fraction of surfactant and the total volume fraction of amphiphile ϕ_S/ϕ.

The derivation of eqs 1−4 was done without any constraint on the composition of the aggregates, and therefore these equations still hold in the case of ϕ being the total amphiphile volume fraction. More attention does have to be given, however, to the *intra*aggregate energy contribution $\epsilon^{\circ,agg}$, now becoming composition-dependent:

$$\epsilon^{\circ,agg}(\phi_S,\phi) = \epsilon^{\circ,agg}\left(\frac{\phi_S}{\phi}=0\right) + \frac{\phi_S}{\phi}\left[\epsilon^{\circ,agg}\left(\frac{\phi_S}{\phi}=1\right) - \epsilon^{\circ,agg}\left(\frac{\phi_S}{\phi}=0\right)\right] \quad (8)$$

with agg again referring alternatively to lam and hex. Note that the condition $\phi_S/\phi = 1$ corresponds to "only surfactant" (limit of W−S mixture) and $\phi_S/\phi = 0$ to "only lipid" (limit of W−L mixture); $\epsilon^{\circ,lam(hex)}((\phi_S/\phi)=0)$ is the energy per molecule of a lipid in a pure lipid bilayer (cylinder), while $\epsilon^{\circ,lam(hex)}((\phi_S/\phi)=1)$ refers similarly to the corresponding pure surfactant energies.

This expression can be further generalized if the entropy of mixing of S and L molecules within each aggregate form is considered. $\epsilon^{agg}(\phi_S,\phi)$ denotes the free energy per molecule in one phase; we can write the total free energy in that aggregate as the weighted average of the free energy per mole of the lipid and the free energy per mole of the surfactant in that phase:

$$\epsilon^{agg} = \frac{\epsilon_L^{agg} N_L + \epsilon_S^{agg} N_S}{N_L + N_S} \quad (9)$$

where N_L and N_S are the number of lipid and surfactant molecules in each aggregate. The analogue of the chemical potential for *surfactant* in the aggregate, for example, is

$$\epsilon_S^{agg} = \epsilon_S^{\circ,agg} + \ln(\phi_S/\phi) \quad (10)$$

Here the standard state ϵ_S° refers to the condition $\phi_S/\phi = 1$, meaning $\phi_L = 0$; *i.e.*, no lipid is present in the aggregate. Combining eq 9 with eq 10 and the analogue of eq 10 for the lipid (ϵ_L^{agg}), we obtain the generalization of eq 8:

$$\epsilon^{agg} = \epsilon_L^{\circ,agg} + \frac{\phi_S}{\phi}[\epsilon_S^{\circ,agg} - \epsilon_L^{\circ,agg}] + \left\{\frac{\phi_S}{\phi}\ln\left(\frac{\phi_S}{\phi}\right) + \left(1-\frac{\phi_S}{\phi}\right)\ln\left(1-\frac{\phi_S}{\phi}\right)\right\} \quad (11)$$

Concentration vs Composition. Now we summarize the overall adimensional free energy per unit volume for lamellar and hexagonal phases and proceed to the calculation of the tie lines for the two-phase region of the phase diagram:

$$\tilde{\psi}^{lam} = x\ln\left(\frac{\Lambda_{lam}}{l}\right) + x\ln\left(\frac{x}{1-x}\right) - x + \epsilon^{lam}x$$

$$\tilde{\psi}^{hex} = x\ln\left(\frac{\Lambda_{cyl}^2}{a}\right) + x\ln\left(\frac{x}{1-x}\right) + \frac{x}{1-x} - 2x + \epsilon^{hex}x \quad (12)$$

Here we have used eqs 2 and 4 and transformed from volume fractions ϕ to mole fractions x, which are identical since all molecular volumes have been taken to be the same. We find it natural to use ϕ for the description of the excluded volume interactions, but now we turn to the calculation of the chemical potentials as number derivatives of the Helmholtz free energy, and the mole fraction becomes the natural unit to use. An equivalent of the common tangent construction is performed by setting the chemical potentials of the three components in the hexagonal phase equal to those in the lamellar phase:

$$\begin{cases} \tilde{\mu}_S^{lam}(x_S^{lam},x_L^{lam}) = \tilde{\mu}_S^{hex}(x_S^{hex},x_L^{hex}) \\ \tilde{\mu}_L^{lam}(x_S^{lam},x_L^{lam}) = \tilde{\mu}_L^{hex}(x_S^{hex},x_L^{hex}) \\ \tilde{\mu}_W^{lam}(x_S^{lam},x_L^{lam}) = \tilde{\mu}_W^{hex}(x_S^{hex},x_L^{hex}) \end{cases} \quad (13)$$

This constitutes a system of three equations in four unknowns: the "extra" degree of freedom provides the equation of the curve specifying the first-order coexistence. Numerical solution of eqs 13 leads to the phase diagram shown in Figure 3. We have chosen for this case $\epsilon_S^{\circ,lam} = 2$, $\epsilon_S^{\circ,hex} = 0$, $\epsilon_L^{\circ,lam} = 0$, and $\epsilon_L^{\circ,hex} = 2$. Note that the absolute energy values of the standard states are not important but rather only their relative values $\Delta\epsilon_S^\circ = \epsilon_S^{\circ,lam} - \epsilon_S^{\circ,hex}$ (=+2 here), and $\Delta\epsilon_L^\circ = \epsilon_L^{\circ,lam} - \epsilon_L^{\circ,hex}$ (=−2).

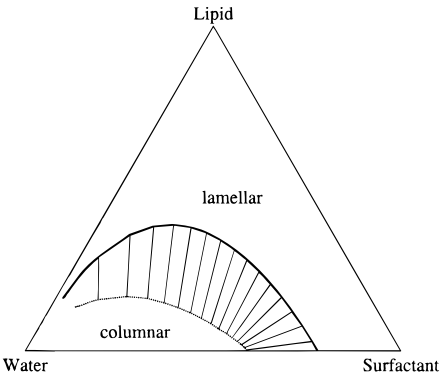

Figure 3. Ternary phase diagram of a water, lipid, and surfactant system, showing phase coexistence between the columnar phase and the lamellar phase.

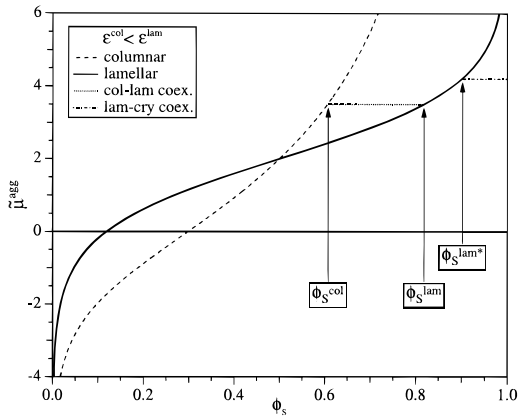

Figure 4. Dimensionless chemical potential $\tilde{\mu}^{agg}$ plotted versus volume fraction of surfactant ϕ_S. "Agg" stands for "lam", lamellar phase, for "col", columnar phase, and for "cry", crystal phase. There are two-phase coexistence regions indicated in the figure: the first one between columnar and lamellar phase and the second one between lamellar and crystal phase. Self-energies $\epsilon°$ are the same as those in the top panel of Figure 2.

(Recall that all energies are measured in units of k_BT and that typical $\Delta\epsilon°$'s are indeed of the order of k_BT.[7])

An important feature of this phase behavior is that the extension of the hexagonal phase toward the lamellar and the broadening of the two-phase region are controlled by variation in the relative values of the standard state ("self-") energies. In addition, each tie line connects two points belonging to the two phase boundaries with realistic compositions. In particular we note that the ratio of x_L/x_S is always larger at the lamellar end point than at the corresponding hexagonal end point. That is, the lamellar phase is always richer in the *non*-curvature-liking amphiphile.

On the other hand, the phase diagram does not represent realistically the two limits of very low and very high concentration. Both lamellar and hexagonal phases are seen to extend to low concentration, whereas one actually expects *neither* of them in these limits. Rather, vesicle and/or micellar phases are observed. Also, at high concentrations the lamellar phase extends in our phase diagram all the way to pure surfactant and pure lipid, whereas one expects it to phase separate there into pure lipid (crystal) and/or pure surfactant (crystal).

Demixing to Pure Components of Amphiphile. We incorporate phase separation to pure crystal states via an upper limit for the value of the chemical potential of surfactant and lipid, corresponding to the appearance of these latter phases. At this boundary, the chemical potential of the amphiphile in the aggregates equals the chemical potential in its pure crystalline form, signalling a first order phase transition: $\tilde{\mu}_S^{lam} = \tilde{\mu}_S^{cry}$. This construction is clarified in Figure 4, where we restrict the analysis to the two-component limit W−S, using the same self-energies $\epsilon°$ as in Figure 5a.[15]

In the more general case of the three-component mixture, an equation like $\tilde{\mu}_S^{lam} = \tilde{\mu}_S^{cry}$ has to be satisfied for lipid species as well:

$$\begin{cases} \tilde{\mu}_S^{lam}(x_S^{lam},x_L^{lam}) = \tilde{\mu}_S^{cry}(x_S^{cry}=1,x_L^{cry}=0) \\ \tilde{\mu}_L^{lam}(x_S^{lam},x_L^{lam}) = \tilde{\mu}_L^{cry}(x_S^{cry}=0,x_L^{cry}=1) \end{cases} \quad (14)$$

The solution to this system of two equations in two unknowns is unique and gives the coordinates of the triple point. At this point, the lamellar phase is in equilibrium with the pure crystal lipid and pure crystal surfactant. The triangle connecting this triple point to the S-vertex and the L-vertex constitutes a three-phase region: see Figure 5a. Each point within the three-phase region is connected to the critical point and to the two vertices by three tie lines.

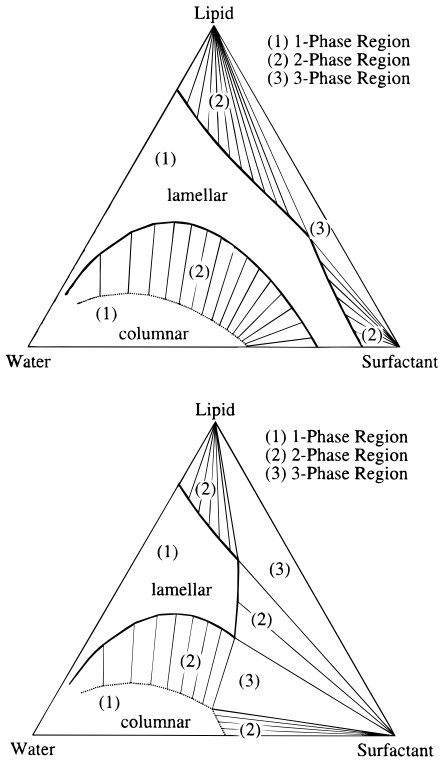

Figure 5. Two possible ternary phase diagrams when the phase coexistence with the pure crystal is taken into account: (a, top) pure lipid crystal and pure surfactant crystal in equilibrium with the lamellar phase; (b, bottom) pure lipid crystal in equilibrium with the lamellar phase only, while pure surfactant crystal is in equilibrium with both phases. Notice the presence of one-, two-, and three-phase regions.

From the triple point depart two other interesting lines, namely, the phase boundaries of the lamellar phase limiting a new two-phase region. We can calculate these lines by equating for example the chemical potential of the surfactant in the lamellar phase with the chemical potential of pure crystal surfactant: $\tilde{\mu}_S^{lam}(x_S^{lam},x_L^{lam}) = \tilde{\mu}_S^{cry}$. This equation in two unknowns describes a curve in a two-dimensional space and specifies the two-phase boundary. Every point within the two-phase region is connected through a tie line to the edge of the lamellar phase and to the pure S vertex. An analogous procedure can be performed for the two-phase equilibrium with pure lipid. The full phase diagram is plotted in Figure 5a, for a typical set of self-energies.[15]

An even more interesting case arises when the calculated lamellar/pure-S boundary line crosses the lamellar−hexagonal boundary line. At the crossing there are three phases at equilibrium: lamellar, hexagonal, and pure S, corresponding to a new triple point. A new three-phase region can be drawn by connecting the new triple point to the conjugated point in the hexagonal phase boundary and to the pure S vertex. Finally, one last phase boundary has to be calculated, namely, hexagonal phase in equilibrium with pure-S, corresponding to which a new two-phase region appears in the lower right-hand corner of the phase diagram: $\tilde{\mu}_S^{hex}(x_S^{hex},x_L^{hex}) = \tilde{\mu}_S^{cry}$. The new phase diagram is plotted in Figure 5b.[15]

Model for the Micellar Phase. The second unrealistic feature expressed by the phase diagram in Figure 3 can be addressed by allowing for the presence of a micellar phase present at very low concentrations of amphiphile.

We exploit once again a hard-particle model for the micellar phase. As far as inter-aggregate/"packing" considerations are

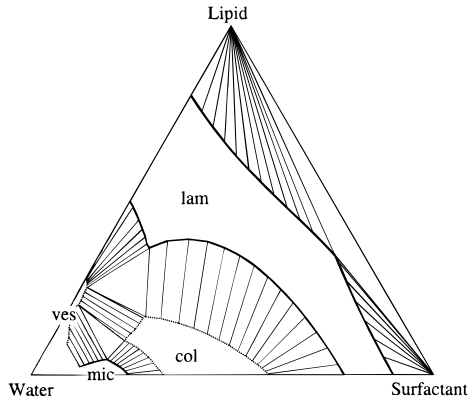

Figure 6. One possible scenario for a ternary phase diagram, in which several phases coexist at equilibrium: "ves", vesicle phase; "mic", micellar phase; "col", columnar phase; "lam", lamellar phase.

concerned, this phase can be thought of as a collection of hard spheres in a 3D space. The spheres are allowed to translate in space with no restrictions, other than to avoid overlap of their hard cores. The three-term truncation of the *y*-expansion gives for the pressure[12]

$$\frac{Pv}{kT} = \frac{\phi}{1-\phi} + 3\left(\frac{\phi}{1-\phi}\right)^2 + 3\left(\frac{\phi}{1-\phi}\right)^3 \qquad (15)$$

where v is the volume of one sphere: note that this result is identical to that obtained from an exact solution of the Percus−Yevick theory,[16] with the compressibility equation for the pressure, and to the scaled particle pressure.[17] Each sphere contains a number of amphiphile molecules, so v does *not* coincide here with *molecular* volume. Integration of eq 15 gives the free energy of the micellar phase:

$$\frac{F(\phi)}{N} = kT\ln\left(\frac{\Lambda_{\mathrm{mic}}{}^3}{v}\right) + kT\ln\left(\frac{\phi}{1-\phi}\right) + kT\frac{3}{2(1-\phi)^2} - \frac{5}{2}kT \qquad (16)$$

where Λ_{mic} is the De Broglie wavelength of the spherical micelle. This result accounts for the inter-aggregate contribution to the overall free energy. The *self*-energy term can be derived exactly in the same way as we did for the hexagonal and lamellar phases.

If we focus first on the micellar and hexagonal phases, we can compute the tie lines for the micellar to hexagonal phase transition for a particular choice of standard states.[15] The micellar phase appears at much lower concentrations than the hexagonal phase and soon becomes unstable. The tie lines within the two-phase region reflect the S and L curvature references: each point in the hexagonal phase contains more lipid than its conjugate point in the micellar phase, consistent with the hexagonal phase having less average curvature than the micellar, while its aggregates pack more efficiently.

Model for the Vesicle Phase. Any lipid which forms a lamellar phase by itself at high enough concentrations will form vesicles, pieces of bilayers, etc., at low volume fractions. We model this state of the system as the "vesicle phase", strictly comprised of a monodisperse solution of spherical vesicles. For purposes of calculating *packing* free energy, these spherical-shell aggregates are no different from filled spheres, except for the shells containing a lot of the solvent; accordingly, the volume fraction of amphiphile making up the shells has to be properly rescaled. This suggests that the hard-particle model for the micellar phase—see, for example, eq 15—can be used also for the vesicle phase, but with v the actual volume occupied by the shell and not the volume contained within it. Integration of the pressure gives the appropriate free-energy—see eq 16 but with the De Broglie wavelength Λ_{ves} corresponding to that of the *shell*. As before the self-energy term can be derived from curvature energy and entropy of mixing arguments, much as in recent treatments of the "vesicle → micelle" transition in the dilute solution limit.[18,19]

Master Phase Diagram. We focus here on the vesicle and lamellar phases, for a particular choice of standard states,[15] computing the tie lines for the vesicle-to-lamellar phase coexistences. The vesicle phase is found to appear at much lower concentrations than the lamellar phase and soon becomes unstable. The presence of some surfactant extends the area of stability of the vesicle phase. A more complete phase diagram makes use of all the pieces of information gathered so far and is shown in Figure 6.[15] It accounts simultaneously for the relative stabilities of micellar, vesicle, hexagonal, lamellar, and pure crystal amphiphile phases, incorporating the self-energy and hard-core packing effects outlined in the previous sections. Still other, more exotic, micellar structures and ordered phases can in principle be treated in a similar way.

Acknowledgment. We are pleased to contribute this paper to the festschrift in honor of our old friend Daniel Kivelson, whom we like and admire very much. Throughout the course of this work we have benefited from stimulating discussions with Avinoam Ben-Shaul and Yardena Bohbot; we thank them heartily for their many valuable suggestions and clarifying remarks. This work is supported in part by Grant CHE 95-20808 from the National Science Foundation.

References and Notes

(1) Israelachvili, J. N.; Mitchell, D. J.; Ninham, B. W. *J. Chem. Soc., Faraday Trans. 1* **1976**, *72*, 1525.
(2) Tanford, C. *The Hydrophobic Effect*; Wiley: New York, 1980.
(3) Gelbart, W. M.; Ben-Shaul, A.; Roux, D. *Micelles, Membranes, Microemulsions, and Monolayers*; Springer-Verlag: New York, 1994.
(4) Smit, B.; *et al. J. Phys. Chem.* **1991**, *95*, 6361.
(5) Larson, R. G. *J. Chem. Phys.* **1992**, *96*, 7904.
(6) Zoeller, N. J.; Shiloach, A.; Blankschtein, D. *Chemtech* **1996** (Mar), 24.
(7) Gelbart, W. M.; Ben-Shaul, A. *J. Phys. Chem*. **1996**, *100*, 13169.
(8) See: Herzfeld, J. *Acc. Chem. Res.* **1996**, *29*, 31, and references cited therein.
(9) Parsegian, V. A. *Trans. Faraday Soc*. **1966**, *62*, 848.
(10) Mather, D. E. *J. Colloid Interface Sci.* **1976**, *57* (2), 240.
(11) Ekwall, P. *Adv. Liq. Cryst.* **1975**, *1*, 1.
(12) Barboy, B.; Gelbart, W. M. *J. Chem. Phys*. **1979**, *71* (7), 3053.
(13) See, for example, discussion surrounding Figure 1.9 in Chapter 1 of ref 3.
(14) Note that eqs 7 are equivalent to imposing the conditions,

$$\begin{cases} \tilde{\mu}_{\mathrm{S}}^{\mathrm{lam}}(\phi_{\mathrm{S}}^{\mathrm{lam}}) = \tilde{\mu}_{\mathrm{S}}^{\mathrm{hex}}(\phi_{\mathrm{S}}^{\mathrm{hex}}) \\ \tilde{\mu}_{\mathrm{W}}^{\mathrm{lam}}(\phi_{\mathrm{S}}^{\mathrm{lam}}) = \tilde{\mu}_{\mathrm{W}}^{\mathrm{hex}}(\phi_{\mathrm{S}}^{\mathrm{hex}}) \end{cases}$$

(15) For the phase diagrams shown in Figures 4, 5a, and 6, we take: $\epsilon_{\mathrm{L}}^{\circ\,\mathrm{lam}} = 0$, $\epsilon_{\mathrm{S}}^{\circ\,\mathrm{lam}} = 2$, $\epsilon_{\mathrm{L}}^{\circ\,\mathrm{col}} = 2$, $\epsilon_{\mathrm{S}}^{\circ\,\mathrm{col}} = 0$, $\epsilon_{\mathrm{L}}^{\circ\,\mathrm{ves}} = -2$, $\epsilon_{\mathrm{S}}^{\circ\,\mathrm{ves}} = 2$, $\epsilon_{\mathrm{L}}^{\circ\,\mathrm{mic}} = 0$, $\epsilon_{\mathrm{S}}^{\circ\,\mathrm{mic}} = -1$, and finally $\epsilon_{\mathrm{L}}^{\circ\,\mathrm{cry}} = 1.4$ and $\epsilon_{\mathrm{S}}^{\circ\,\mathrm{cry}} = 4.2$. The phase diagram in Figure 5b involves the same set of self-energies, except for $\epsilon_{\mathrm{S}}^{\circ\,\mathrm{cry}} = 2.4$.
(16) Percus, J. K.; Yevick, G. J. *Phys. Rev*. **1958**, *110*, 1.
(17) Reiss, H.; Frisch, H. L.; Lebowitz, J. L. *J. Chem. Phys.* **1959**, *31*, 369.
(18) Andelman, D.; Kolzov, M. M.; Helfrich, W. *Europhys. Lett*. **1994**, *25*, 231.
(19) Fattal, D. R.; Andelman, D.; Ben-Shaul, A. *Langmuir* **1995**, *11*, 1154.